Reaction Kinetics, Mechanisms and Catalysis (2024) 137:1771–1787
https://doi.org/10.1007/s11144-024-02610-4

Green synthesis of ZnO-doped cerium oxide nanocomposite using clove extract: enhanced photocatalytic methylene blue degradation and antibacterial properties

Brahim Djemoui[1] · Samia Gharbi[2] · Choukry Kamel Bendeddouche[1] · Zohra Taibi[3] · Miloud Mohamed Mazari[1] · Abdelhalim Zoukel[4] · Noureddine Karkachi[5] · Mehdi Adjdir[1,6]

Received: 29 February 2024 / Accepted: 11 March 2024 / Published online: 19 March 2024

Abstract

In this study, we present a green synthesis method for producing ZnO-doped CeO_2 nanocomposites (ZnO–CeO_2 NC) and CeO_2 nanoparticles (NPs) using clove (*Syzygium aromaticum*) extract. Our main objective is to assess their properties, focusing on their photocatalytic and antibacterial activities. Through comprehensive characterization techniques such as powder XRD, UV–vis DRS, and FTIR analyses, we thoroughly evaluated the synthesized materials. Notably, both the green-synthesized CeO_2 (CLV30) NPs and ZnO–CeO_2 (CZn) NCs demonstrated exceptional efficiency, degrading methylene blue dye by 89% and 94%, respectively, under visible light irradiation. The CZn nanocomposites exhibited remarkable reusability and stability over four cycles. Additionally, significant antibacterial activity was observed, with CLV30 exhibiting moderate effectiveness against Gram-negative *Escherichia coli* (*E. coli*) (8 mm) and Gram-positive *Staphylococcus aureus* (*S. aureus*) (11 mm) compared to CZn, which displayed notable inhibitory zones of 24 mm and 35 mm against *E. coli* and *S. aureus*, respectively. These findings highlight the versatile applications of these nanomaterials across various fields.

Keywords Cerium oxide nanoparticles · Green synthesis · ZnO-doped CeO_2 nanocomposites · Photocatalytic activity · Antibacterial properties · Syzygium aromaticum extract

Introduction

Currently, industrial, laboratory, and medical pollutants pose significant threats to human health and the environment by directly entering water bodies, disrupting marine systems, and exacerbating global drinking water scarcity [1, 2]. Water

Extended author information available on the last page of the article

contamination from dyes in industrial wastewater, originating from sectors such as textile dyeing, papermaking, food processing, paints, and cosmetics, is a notable contributor to aqueous pollution [3, 4]. To address this issue, various techniques, including biological microorganisms like bacteria [5], fungi[6], algae [7], yeast cells [8] and chemical processes such as chlorination[9], precipitation[10], ion exchange[11], photocatalysis[12–14], adsorption [15] are employed for wastewater treatment. Among these methods, photocatalytic dye degradation stands out as a promising approach for pollutant removal [16]. Nanoscience has played a crucial role in offering a practical solution by facilitating the development of a safe, cost-effective, and biocompatible answer to the problem. The biosynthesis of metal and metal oxide nanoparticles (NPs) using plant extracts represents a groundbreaking area in nanobiotechnology, grounded in the principles of green chemistry [17, 18].

Cerium oxide (CeO_2) succeeded in receiving the attention of many in the fields of medicine and industry, due to being capable of converting state Ce^{3+} into Ce^{4+} and vice versa and containing oxygen holes in its crystal structure [19]. Cerium is a gray metal element that belongs to the group of lanthanides. It has consisted of oxide salt with a crystallized structure that is face-centered cubic (fcc) with an Fm3m space group [20, 21]. The unique physical and chemical properties of CeO_2 led to its exertion in many applications throughout various fields, including catalyst [22] photocatalysis [23], biomedicine [24], optical devices [25], oxygen sensor [26]. There are several methods for the fabrication of CeO_2 NPs such as co-precipitation [27], thermal-hydrolysis [28], hydrothermal [29], microwave [30], solvothermal [31], and sol–gel [32].

The focus has shifted towards an environmentally friendly green synthesis approach. In this method, biological agents such as plant extracts, bacteria, fungi, algae, and yeasts are employed. Notably, all these agents are biodegradable and do not generate toxic compounds during the synthesis process [33, 34]. The choice of an appropriate capping agent is recognized as a critical factor influencing the size, morphology, and structure of synthesized nanoparticles (NPs). Green nanotechnology, utilizing renewable resources, has the potential to decrease energy consumption. Overall, enhancing energy efficiency, minimizing the use of non-renewable materials, and lowering greenhouse gas emissions stand out as key advantages of adopting a green synthesis approach for nanomaterials [35].

Hence, *Syzygium aromaticum*, commonly known as clove, is a medium-sized tree (8–12 m) belonging to the Myrtaceae family and native to the Maluku islands in east Indonesia [36]. Clove contains up to 18% essential oil, with eugenol comprising approximately 89%, and eugenol acetate and β-caryophyllene making up 5% to 15% [37]. Eugenol, identified as the predominant compound in clove essential oil, exhibits notable antibacterial, antioxidant, and insecticidal properties. Recognized by the Food and Drug Administration as a natural food additive generally regarded as safe [38], clove serves a dual purpose in food applications. Beyond imparting flavor, it acts as a preservative, leveraging its antioxidant and antibacterial attributes. Specifically, clove extract, rich in Eugenol, functions as a preservative, safeguarding against foodborne pathogens and spoilage [39].

Therefore, the main goals of this investigation were to evaluate the feasibility of employing clove extract in the synthesis of both cerium oxide (CeO_2) nanoparticles

and their zinc-doped counterparts. The aim was to optimize synthesis conditions to produce CeO_2 nanoparticles and ZnO–CeO_2 nanocomposites with enhanced photochemical and biological properties. The investigation encompassed assessing antibacterial activity against two bacterial strains, namely Gram-positive *Staphylococcus aureus* (*S. aureus*) and Gram-negative *Escherichia coli* (*E. coli*). Additionally, it aimed to assess the photocatalytic efficacy in degrading methylene blue dye from water.

Materials and methods

Materials

All chemical substances employed in this study were acquired with a notably high degree of purity. Cerium (IV) sulfate ($Ce(SO_4)_2$), Zinc chloride ($ZnCl_2$), and Methylene blue dye were sourced from Merck, ensuring stringent quality standards. Fresh clove powder was procured from a reputable herbal shop in Oran, Algeria. Distilled water served as both the solvent and the medium for preparing the dye solution, facilitating the precise execution of the adsorption experiment.

Preparation of the clove extract

To obtain the clove extract, 10 g of finely powdered clove was introduced into 100 mL of distilled water, undergoing a controlled boiling phase at 80 °C for a duration of 15 min Subsequent to this thermal treatment, the resultant solution underwent filtration, with the clear filtrate carefully collected and stored in a dark vial. For optimal preservation, the vial was then placed in a refrigerated environment at 4 °C.

Synthesis of CeO_2 NPs and Zn doped CeO_2 NC

In order to synthesize CeO_2 NPs, 2 g of $Ce(SO_4)_2$ was dissolved in distilled water and stirred until achieving a clear yellow solution. Subsequently, clove extract was incrementally added in varying volumes according to ratios of 90:10, 80:20, and 70:30, with the addition carried out dropwise. The color of the $Ce(SO_4)_2$ solution transitioned from yellow to beige upon complete addition of the clove extract. The pH of the solution was adjusted to a value of 9 utilizing 5M NaOH to ensure proper alkalinity, the solution assumed a dark brown color. The resulting solutions were designated as CLV10, CLV20, and CLV30, and were subjected to continuous stirring for 24 h at room temperature.

For the synthesis of the ZnO–CeO_2 NC, 1 g of $ZnCl_2$, constituting 20% by weight of $Ce(SO_4)_2$, was introduced into the CLV30 solution and labeled as CZn. Subsequently, the solutions underwent filtration, and the resultant solids were thoroughly washed with distilled water, followed by a final wash with ethanol. The washed solids were then dried in an oven at 60 °C and subjected to calcination at 600 °C for a duration of 1 h.

Photocatalytic activity study

The photocatalytic performance of the green synthesized CLV30 NPs and CZn NCs was evaluated by the degradation of Methylene blue (MB) dye in aqueous solution under visible-light irradiation with a 30 W LED lamp. The concentration of the stock solution of MB is 10 mg/L. the 10 mg NCs mixed with 20 mL of MB dye solution. This mixture was left in the dark for 30 min while being stirred. The dark environment aids in the establishment of the adsorption–desorption equilibrium phase. The light irradiated NCs solutions were taken out (3 mL in every 30 min) to evaluate the absorbance from UV spectroscopy. The samples were centrifuged to remove the solid NCs from the dye solution before calculate the absorbance.

The dye degradation efficiency was determined using the equation below [40],

$$D(\%) = \frac{A_0 - A_t}{A_0} \times 100$$

Here A_0 and A_t represent the initial absorbance before Visible-Light irradiation and the absorbance of the solution at time t, respectively.

Antibacterial activity

The antibacterial activities of the synthesized CLV10, CLV20 and CLV30 NPs and CZn NC were tested against Gram-positive *Staphylococcus aureus* (*S. aureus*) and Gram-negative *Escherichia coli* (*E. coli*) bacterial strains using the disc diffusion method. The Muller-Hinton broth was used to establish bacterial growth for 24 h [41]. Bacteria that had been cultured and isolated were streaked into sterilized petri plates (bacterial culture = 10^{-6} CFU/mL). 10 mg of the synthesized CLVs NPs and CZn NC were placed onto 6 mm paper discs. The loaded discs were put in a 37 °C incubator overnight. Lastly, the inactivation of bacterial strains was determined by measuring the zone of the inhibition on a millimeter's scale.

Characterization

A variety of analytical techniques were utilized to investigate the morphology, chemical composition, and functional groups of CeO_2 NPs as well as the ZnO–CeO_2 NC. The Fourier Transform Infrared Spectroscopy (FTIR) spectrum was recorded at room temperature using KBr pellet on a JASCO FT/430 spectrophotometer between 400 and 4000 cm^{-1} facilitated the examination of functional groups within both the CeO_2 NPs and the ZnO–CeO_2 NC, JASCO V-460 UV–Vis spectrophotometer was used to collect the diffuse reflectance spectra (DRS) were captured within the wavelength range of 200–800 nm with a resolution of 0.2 nm conducted to investigate the synthesized nanomaterials optical absorption properties, and The X-ray powder diffraction (XRD) spectrum was registered by a BRUKER D8 Apparatus

diffractometer with Cu Kα radiation (0.15418 nm wavelength). Data were collected in the 2θ degree range of 2°–80°, with a step size of 0.02◦, the XRD pattern provided insights into the crystalline structure of both the CeO_2 NPs and the ZnO–CeO_2 NC.

Results and discussion

Fourier-transform infrared spectroscopy analysis

FTIR spectra of CLV10, CLV20 and CLV30 NPs and CZn NC are shown in Fig. 1. In literature, the broad absorption in the frequency band 3400 cm^{-1} are assigned to O–H stretching from water or Ce-OH [42]. From our result, the band at 1622 cm^{-1} has been attributed to the bending vibration of adsorbed water molecules [43], Moreover, the absorption band at about 1000 cm^{-1} to 1100 cm^{-1} are belong to the characteristic vibration of CeO_2. The band between 400 and 700 cm^{-1} were assigned to M–O (M = Zn, Ce) stretching vibrations [22, 44].

X-ray diffraction patterns

XRD patterns of green synthesized CeO_2 NPs and Zn-CeO_2 NCs are shown in Fig. 2. The pure green synthesized CLV10, CLV20, and CLV30 NPs at 2 theta i.e. 28.6°, 33.15°, 47.55°, 56.4°, 59.2°, 69.55°, 76.75° and 79.2° correspond to the (hkl) planes of (111), (200),(311),(222),(400),(331) and (420) [45].The absence of new peaks confirmed the phase purity of the face centered cubic structure of the green synthesis CeO_2 NPs which exactly matches the JCPDS data card no: 03-065-5923. The new peaks 2 theta = 31.78°, 34.44°, 36.27°, 47.53°, 56.59° and 62.87° correspond to the (hkl) planes of (100), (002), (101), (102), (110) and (103), respectively matches the JCPDS data card no: 01-079-2205 represent the hexagonal crystal of zinc oxide. The average crystallite size of the

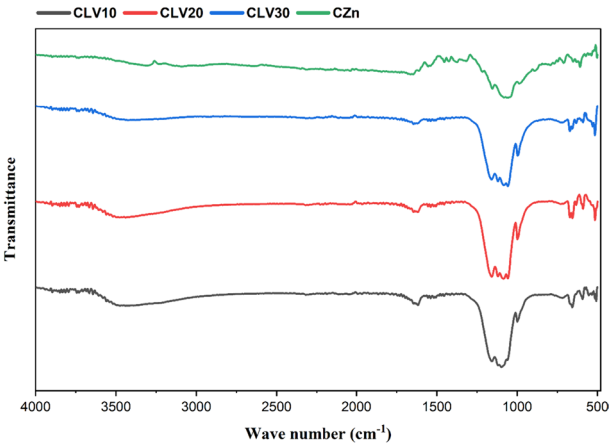

Fig. 1 FTIR spectra of the synthesized CeO_2 (CLVs) NPs and ZnO–CeO_2 (CZn) NC

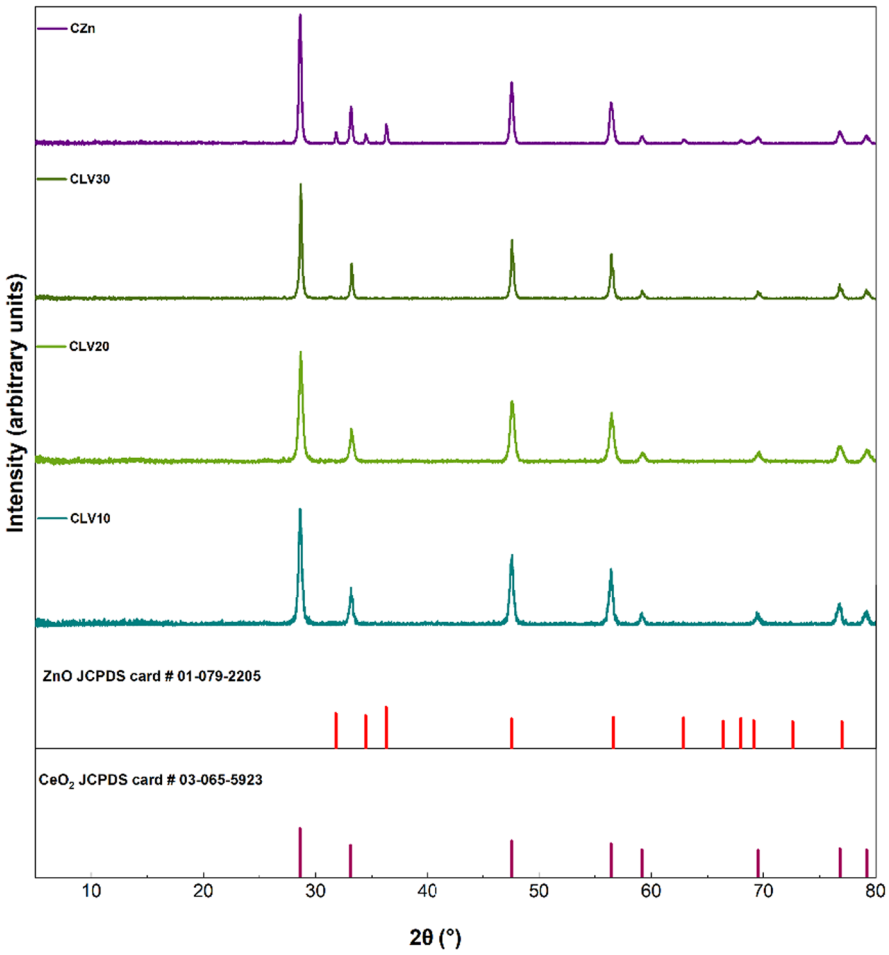

Fig. 2 Powder X-ray diffraction patterns of synthesized CLVs NPs and CZn NC

green synthesized CLV10, CLV20, and CLV30 NPs and CZn NC were calculated by Scherrer's formula: $D = k\lambda/\beta \cos\theta$ [46]. The obtained average crystallite size values are 16 nm, 13 nm, 20 nm and 28 nm respectively, In the realm of green synthesis, Mahmoodi et al. [40] reported an average crystallite size of CeO_2 NPs of 45 nm using zucchini peel extract, suggesting a comparable methodology. Additionally, Parvathy et al. [47] employed *Artabotrys hexapetalus* leaf extract and observed an average crystallite size of 60 nm of CeO_2 NPs. Notably, Ahmed et al. [48] and Anvarinezhad et al. [49] reported average crystallite sizes of 30 nm for CeO_2 NPs from *Artabotrys hexapetalus* leaf extracts and 50 nm for ZnO NPs from hydroalcoholic clove extract, providing valuable context and insights into similar green synthesis approaches.

UV–vis DRS spectroscopy analysis

The ultraviolet–visible (UV–vis) diffuse reflectance spectra of CLV30 and CZn photocatalysts are presented in Fig. 3a, with CZn exhibiting a shift towards the visible region at the 380 nm band compared to CLV30. Band gap energy (Eg) was determined utilizing the formula $E = 1240/\lambda_{\text{Absorp.Edge}}$ and $(\alpha h\nu)^{2/n}$ [50, 51].

Optical characterization was performed using a UV–vis absorption spectrophotometer across the 200–800 nm wavelength range. Results indicate potential applications of both composite and pure materials in the visible light region.

The band gap energy of a semiconductor can be computed using Eq. 1:

$$\alpha h\nu = A\left(h\nu - E_g\right)^{n/2} \tag{1}$$

Here α represents the absorption coefficient, h denotes Planck's constant, ν stands for light frequency, Eg signifies band gap energy, and A is the proportionality constant. The exponent n is determined by the type of optical transition (n = 1 for direct transition and n = 4 for indirect transition). The plots of $(\alpha h\nu)^{2/n}$ versus photon energy (hν) were employed to estimate the band-gap energy (Eg) of the samples [52].

Analysis of $(\alpha h\nu)^{2/n}$ versus (hν) plots yielded band gap values of 2.78 eV for CLV30 and 2.8 eV for CZn photocatalysts, as depicted in Fig. 3b. Notably, the CZn photocatalyst exhibited a slightly larger band gap energy compared to CLV30 (2.78 eV).

Photocatalytic activity

In the course of the photocatalytic experiments, UV–vis absorption analysis was employed to examine the degradation of methylene blue dye (10 mg/L) by the prepared materials. Before initiating the photocatalytic tests, attaining adsorption–desorption equilibrium was crucial. This required agitating the pre-synthesized catalysts with the targeted pollutant under dark conditions for specific predetermined

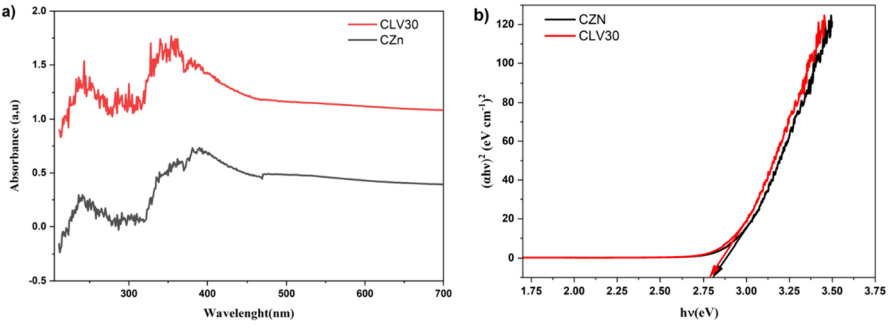

Fig. 3 **a** UV–vis absorbance spectra, and **b** band gap energy of the synthesized CLV30 NPs and CZn NC

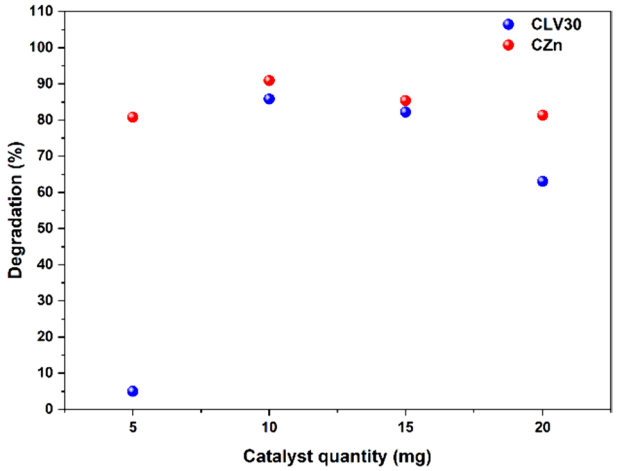

Fig. 4 Effect of catalyst quantity on MB dye degradation under 30 W LED lamp with 10 mg/L dye concentration

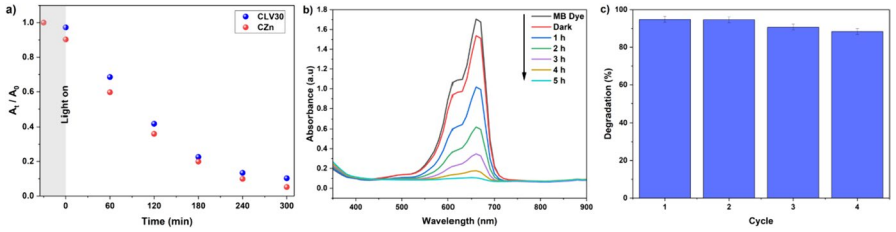

Fig. 5 **a** Photocatalytic degradation curves for MB dye of CLV30 and CZn under visible light; **b** Absorption spectra of MB dye in the presence of CZn during degradation process; **c** Reusability assessment of CZn for the photodegradation of MB dye Experimental conditions include an initial MB concentration of 10 mg/L, a catalyst dosage of 50 mg, a solution volume of 100 mL, and illumination by a 30W LED lamp

durations. These durations were adjusted according to the nature of the pollutant under investigation.

Different quantities of catalysts were utilized, including 5 mg, 10 mg, 15 mg, and 20 mg, in order to determine the optimal weights. As depicted in Fig. 4, the optimal weight for both catalysts CLV30 and CZn was found to be 10 mg.

The performance of the materials in the photocatalytic degradation of MB dye was evaluated, as depicted in Fig. 5a. CZn NC exhibited the highest photocatalytic efficiency, achieving a remarkable 94% degradation of MB dye. This outcome surpassed the performance of the CLV30 nanoparticle, which attained an 89% degradation after 5 h of visible light irradiation. Notably, the experiment was conducted three times to ensure the repeatability of the results. Additionally, it is noteworthy that both CLV30 and CZn demonstrated low adsorption affinity for MB dye, with percentages of 2.77% and 9.71%, respectively. The kinetics of MB

Table 1 Photocatalytic degradation kinetic parameters of MB dye obtained via non-linear least squares fitting for CLV30 NPs and CZn NCs at room temperature

Catalyst	K (min^{-1})	Standard error	R^2
CLV30	0.0063	0.0004	0.9940
CZn	0.0065	0.0002	0.9989

Table 2 Comparison of the present photocatalytic degradation of MB dye with the reported literature

Catalyst	Reaction time (h)	Degradation %	Ref
Co doped CeO_2	6	96	[54]
Cu doped CeO_2	6	97	[55]
Ce doped ZnO	5	65.8	[56]
$CoFe_2O_4$/BiOBr	6	68	[57]
CLV30	5	89	This study
CZn	5	94	This study

dye's photodegradation kinetics in the presence of CLV30 and CZn was conducted through the utilization of the nonlinear least squares approach, employing the equation: $A = X * e^{(-k*t)} + E$ [53]. In this context, X signifies the amplitude, k denotes the pseudo-first order rate constant, and E represents the endpoint. The comprehensive presentation of the relevant data is provided in Table 1. The present MB dye degradation studies were compared with the recent literature and summarized in Table 2 [54–57].

The UV–vis absorption spectra captured during the photocatalytic degradation process of MB dye are depicted in Fig. 5b. Over the course of the reaction, there is a gradual decline in the absorption intensity of MB, indicative of its progressive decomposition and the complete removal of the chromophore group within the MB dye molecule [58]. Notably, throughout the experiment, the characteristic peak corresponding to the MB dye remains unchanged in position, albeit with a diminishing intensity, suggesting the absence of any additional chromophoric by-products [59]. Furthermore, the absence of any new peaks emerging in the UV–vis spectra at the conclusion of the experiments underscores the complete degradation of MB without the formation of intermediates [60].

The suggested mechanism for the photocatalytic disintegration of MB when subjected to visible light irradiation within the current framework can be outlined as follows: When exposed to visible light, the energy of photons surpasses the band gaps of both the CLV30 and CZn semiconductor catalysts, leading to the generation of electron–hole pairs (Eq. 2). These pairs serve as potent reducing and oxidizing agents, respectively. Subsequently, the interaction between oxygen molecules adsorbed on the catalyst surface and the excited electrons in the conduction band yields superoxide radical anions ($^{\cdot}O_2^-$) (Eq. 3), which undergo protonation to yield hydroperoxyl radicals ($^{\cdot}HO_2$) (Eq. 4). These radicals further convert into hydrogen

peroxide (H_2O_2) and hydroxyl radicals ($^{\cdot}OH$) (Eq. 5). The resultant hydroxyl radicals ($^{\cdot}OH$) (Eq. 6) initiate the degradation of the organic dye MB into water (H_2O) and carbon dioxide (CO_2) (Eq. 7). Additionally, water or hydroxide ions on the surface of CZn photocatalysts react with the holes in the valence band to produce hydroxyl radicals ($^{\cdot}OH$), thereby contributing to the degradation process of the dye. Ultimately, the organic contaminants undergo decomposition into CO_2, H_2O, or degradation products [61–64].

The following equations provide a clear understanding of the photocatalytic mechanism:

$$\mathrm{CZn} + \mathrm{light}(h\nu) \rightarrow \mathrm{CZn}(e_{\mathrm{CB}}^{-}) + \mathrm{CZn}(h_{\mathrm{VB}}^{+}) \tag{2}$$

$$\mathrm{CZn}\left(e_{\mathrm{CB}}^{-}\right) + \mathrm{O_2} \rightarrow \mathrm{CZn} + {}^{\cdot}\mathrm{O_2^{-}} \tag{3}$$

$${}^{\cdot}\mathrm{O_2^{-}} + \mathrm{H_2O} \rightarrow \mathrm{HO_2^{\cdot}} + \mathrm{H^{+}} \tag{4}$$

$$\mathrm{HO_2^{\cdot}} + \mathrm{H_2O} \rightarrow \mathrm{OH^{\cdot}} + \mathrm{H_2O_2} \tag{5}$$

$$\mathrm{H_2O_2} \rightarrow 2\,{}^{\cdot}\mathrm{OH} \tag{6}$$

$$\mathrm{OH^{\cdot}} + \mathrm{MB} \rightarrow \text{degradation products} + \mathrm{CO_2} + \mathrm{H_2O} \tag{7}$$

The evaluation of the stability and reusability of the catalysts are important indicators to estimate the performance of photocatalysts. The stability of the synthesized ZnO–CeO_2 NC was studied by four recycling experiments under visible light irradiation, which are shown in Fig. 5c. After each run, the ZnO–CeO_2 NC was washed and dried at 80 °C for 1 h. Fig. 4c shows the photocatalytic efficiency of MB dye was constant and achieved 88% degradation of the dye solution after its 4th cycle. There was a slight decrement in the efficiency of the photodegradation. Therefore, it can be suggested that the ZnO–CeO_2 NC is stable and potential scalability under sunlight irradiation and has the ability to be reused up to 4th cycle.

Antibacterial activity

The antibacterial efficacy of the synthesized CLV10, CLV20, and CLV30 NPs and the CZn NC was assessed through antibacterial activity tests. The results revealed significant inhibitory effects on the growth of both Gram-negative *Escherichia coli* (*E. coli*) and Gram-positive *Staphylococcus aureus* (*S. aureus*). These findings, depicted in Fig. 6, underscore the materials' effectiveness in combating bacterial strains prevalent in such settings. Table 3 provides zone of inhibition values (in millimeters) for CLV10, CLV20, CLV30, and CZn, emphasizing their distinct antibacterial activities against the tested bacterial strains. In particular, the CLV10, CLV20, and CLV30 NPs exhibited varying degrees of efficacy against both *E. Coli* and *S. aureus*. CLV10 demonstrated a zone of inhibition measuring 7 mm and 10

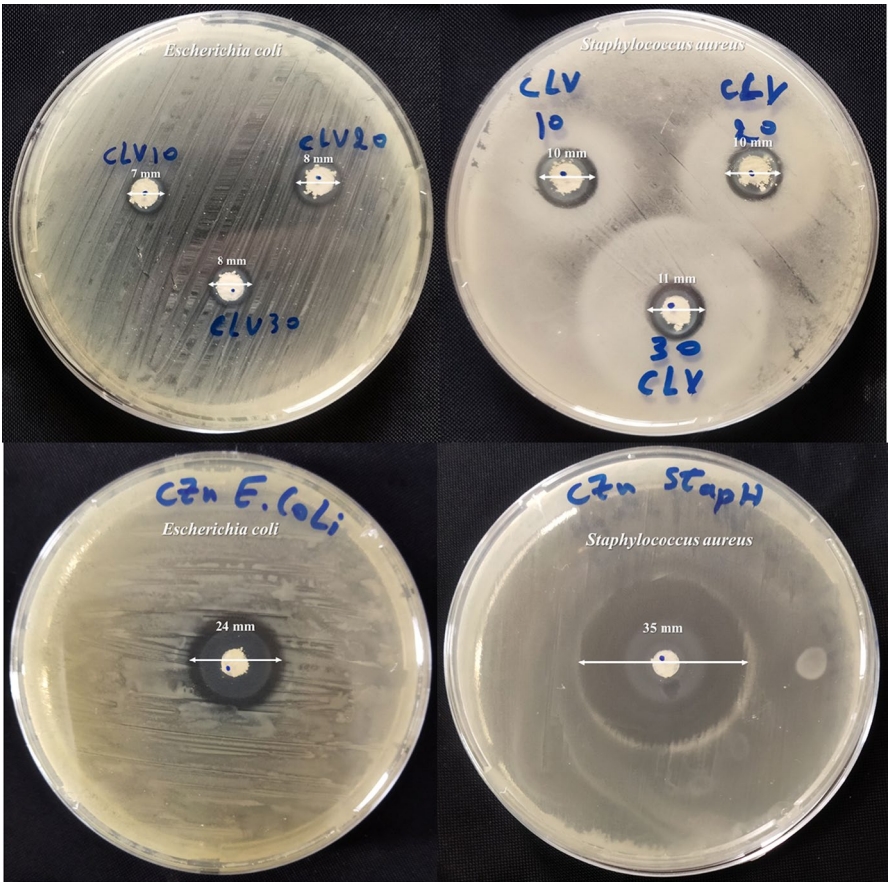

Fig. 6 Assessment of the antimicrobial activity of CLV10, CLV20, and CLV30 nanoparticles (NPs), along with CZn nanocomposite (NC), against *E. coli* and *S. aureus*, depicted by the inhibition zone diameters observed at a dosage of 10 mg

Table 3 Zone of inhibition for CLV10, CLV20 and CLV30 NPs and CZn against *E. coli* and *S. aureus*

Materials		Zone of inhibition (mm) for bacteria	
		E. coli	*S. aureus*
CeO_2	CLV10	7	10
	CLV20	8	10
	CLV30	8	11
$ZnO–CeO_2$	CZn	24	35

mm against *E. Coli* and *S. aureus*, respectively. CLV20 displayed slightly enhanced inhibitory activity with values of 8 mm and 10 mm against the respective bacteria. Furthermore, CLV30 exhibited increased potency, with zone of inhibition

measurements of 8 mm for *E. Coli* and 11 mm for *S. aureus*. The CZn NC exhibited notable antibacterial performance, presenting substantial inhibitory zones of 24 mm and 35 mm against *E. Coli* and *S. aureus*, respectively. This substantial increase in the inhibitory effect compared to the CeO_2 NPs underscores the enhanced antibacterial potential conferred by the incorporation of zinc into the CeO_2 NPs. The green-synthesized CeO_2 NPs and ZnO–CeO_2 NC, positively charged, interacted with negatively charged bacterial strains. This interface-induced electrostatic attractions, resulting in disruptions to the bacterial cell wall. The compromised cell wall facilitated the entry of nanomaterials into the cellular interior, initiating the generation of reactive oxygen species. This intrusion into the cell interior altered DNA and protein synthesis, along with electron chain functions, ultimately impeding nutrient transport and promoting cellular deactivation [65–67].

The results indicate that both CeO_2 NPs and the ZnO–CeO_2 NC exhibit potential as antibacterial agents when compared to previously documented findings in Table 3. Notably, the ZnO–CeO_2 NC demonstrates particularly robust antibacterial activity. The observed differences in efficacy among the CeO_2 NPs underscore the influence of synthesis parameters on antibacterial performance. In summary, these findings offer valuable insights into the prospective application of these nanomaterials for addressing bacterial infections, particularly in aquatic environments (Table 4).

Conclusion

In summary, our study achieved successful synthesis of CeO_2 NPs and ZnO-doped CeO_2 NC through a straightforward, resilient, and environmentally friendly method. The clove extract functioned as a capping agent, effectively reducing the average crystallite size of CeO_2 NPs to 20nm and ZnO–CeO_2 NC to 28nm, as indicated by the Scherrer equation derived from XRD plot results. Antibacterial evaluations revealed reasonable activity for CeO_2 NPs (CLV10, CLV20, and CLV30), with zone of inhibition values ranging from 7 to 11 mm against both *E. coli* and *S. aureus*.

Table 4 Comparative assessment of the antibacterial efficacy of CeO_2 NPs and ZnO–CeO2 NC against *E. coli* and *S. aureus* in comparison with other studies

Materials	Diameter of zone of inhibition (mm) of strain		References
	E. coli	*S. aureus*	
CeO_2	4	5.33	[42]
CeO_2	12	–	[4]
ZnO–CeO_2–Yb_2O	14	13	[68]
$Cu_{0.05}$–$Al_{0.15}$–LDHs	19	15	[41]
CeO_2	15	22	[69]
CeO_2 (CLV10, CLV20 and CLV30)	7,8,8	10,10,11	Present work
ZnO–CeO_2(CZn)	24	35	

Notably, doping CeO_2 (CLV30) with Zinc to form ZnO–CeO_2 NC significantly enhanced antibacterial efficacy, resulting in extraordinary zone of inhibition values of 35 mm and 24 mm against Gram-positive *Staphylococcus aureus* and Gram-negative *Escherichia coli*, respectively. Furthermore, ZnO–CeO_2 NC exhibited remarkable photocatalytic activity, achieving 94% degradation of methylene blue, coupled with stability and reusability over four cycles. These results underscore the potential of our synthesized nanomaterials for applications in antibacterial and photocatalytic processes.

Acknowledgements We extend our sincere appreciation to Dr. Nor el Houda Goual and Dr. Chakib Alaoui for their invaluable support and assistance. Additionally, the corresponding author expresses gratitude to all individuals who have contributed to this work, from its inception to its eventual publication.

Author contributions Conceptualization and Methodology: Brahim Djemoui, Mehdi Adjdir; Formal analysis: Zohra Taibi, Abdelhalim Zoukel; Writing—original draft preparation: Brahim Djemoui; Writing—review and editing: Mehdi Adjdir, Choukry Kamel Bendeddouche, Miloud Mohamed Mazari, Samia Gharbi, Noureddine Karkachi; Investigation: Brahim Djemoui, Mehdi Adjdir; Resources: Samia Gharbi, Noureddine Karkachi; Supervision: Mehdi Adjdir. All authors read and approved the final manuscript.

Funding No funding was received for conducting this study.

Data Availability This article provides data that supports the findings of this study, including supplemental materials. If needed, the corresponding author can provide other relevant data.

Declarations

Conflict of interest The authors declare no competing interests.

References

1. Gharagozlou M, Bayati R (2015) Photocatalytic characteristics of single phase Fe-doped anatase TiO_2 nanoparticles sensitized with vitamin B12. Mater Res Bull 61:340–347. https://doi.org/10.1016/j.materresbull.2014.10.043
2. Li X, He F, Wang Z, Xing B (2022) Roadmap of environmental health research on emerging contaminants: inspiration from the studies on engineered nanomaterials. Eco-Environ Health 1:181–197. https://doi.org/10.1016/j.eehl.2022.10.001
3. Ayodhya D, Ambala A, Balraj G et al (2022) Green synthesis of CeO2 NPs using *Manilkara zapota* fruit peel extract for photocatalytic treatment of pollutants, antimicrobial, and antidiabetic activities. Results Chem 4:100441. https://doi.org/10.1016/j.rechem.2022.100441
4. Vinutha SA, Meghashree AM, Gurudutt DM et al (2023) Facile green synthesis of cerium oxide nanoparticles using *Jacaranda mimosifolia* leaf extract and evaluation of their antibacterial and photodegradation activity. Mater Today Proc 89:105–112. https://doi.org/10.1016/j.matpr.2023.05.592
5. Garg N, Garg A, Mukherji S (2020) Eco-friendly decolorization and degradation of reactive yellow 145 textile dye by *Pseudomonas aeruginosa* and *Thiosphaera pantotropha*. J Environ Manag 263:110383. https://doi.org/10.1016/j.jenvman.2020.110383
6. Noman E, Al-Gheethi A, Talip BA et al (2021) Decolourization of dye wastewater by A Malaysian isolate of *Aspergillus iizukae* 605EAN strain: a biokinetic, mechanism and microstructure study. Int J Environ Anal Chem 101:1592–1615. https://doi.org/10.1080/03067319.2019.1686146
7. Lebron YAR, Moreira VR, Santos LVS (2019) Studies on dye biosorption enhancement by chemically modified *Fucus vesiculosus*, *Spirulina maxima* and *Chlorella pyrenoidosa* algae. J Clean Prod 240:118197. https://doi.org/10.1016/j.jclepro.2019.118197

8. Ledakowicz S, Paździor K (2021) Recent achievements in dyes removal focused on advanced oxidation processes integrated with biological methods. Molecules 26:870. https://doi.org/10.3390/molecules26040870
9. Gunasekaran R, Kanmani S (2014) Performance of gas chlorination in decolourization of textile dyeing wastewater: a pilot study. Clean Technol Environ Policy 16:601–607. https://doi.org/10.1007/s10098-013-0656-9
10. Liu Y, Xu D, Wang P, Dong Y (2016) Removal of sodium salts and chemical oxygen demand from real reactive dye wastewater by the integrated process of chemical precipitation and extraction. Desalin Water Treat 57:6772–6780. https://doi.org/10.1080/19443994.2015.1010232
11. Joseph J, Radhakrishnan RC, Johnson JK et al (2020) Ion-exchange mediated removal of cationic dye-stuffs from water using ammonium phosphomolybdate. Mater Chem Phys 242:122488. https://doi.org/10.1016/j.matchemphys.2019.122488
12. Bernaoui CR, Bendraoua A, Zaoui F et al (2022) Synthesis and characterization of $NiFe_2O_4$ nanoparticles as reusable magnetic nanocatalyst for organic dyes catalytic reduction: study of the counter anion effect. Mater Chem Phys 292:126793. https://doi.org/10.1016/j.matchemphys.2022.126793
13. Goual NEH, Alaoui C, Bendraoua A et al (2023) Petroleum sludge ash-derived MCM-41-silver nanocomposites for enhanced photocatalysis and antimicrobial effect in water treatment. New J Chem 47:20900–20909. https://doi.org/10.1039/D3NJ03613H
14. Chakib A, Bekka A, Mohamed K et al (2022) Sol-gel synthesis of TiO_2/WO_3 and TiO_2/WO_3-graphene nanoparticles, investigation of their photocatalytic proprieties. Chemistry. https://doi.org/10.26434/chemrxiv-2022-khqgj
15. Draoua Z, Harrane A, Adjdir M (2021) Preparation, characterization and application of the nanocomposite PCL-PEG-PCL/bentonite for the removal of methylene blue (MB) dye. Res Chem Intermed 47:4635–4655. https://doi.org/10.1007/s11164-021-04549-w
16. Dong Q, Chen Z, Zhao B et al (2022) In situ fabrication of niobium pentoxide/graphitic carbon nitride type-II heterojunctions for enhanced photocatalytic hydrogen evolution reaction. J Colloid Interface Sci 608:1951–1959. https://doi.org/10.1016/j.jcis.2021.10.161
17. Prabhu D, Arulvasu C, Babu G et al (2013) Biologically synthesized green silver nanoparticles from leaf extract of *Vitex negundo* L. induce growth-inhibitory effect on human colon cancer cell line HCT15. Process Biochem 48:317–324. https://doi.org/10.1016/j.procbio.2012.12.013
18. Hebbalalu D, Lalley J, Nadagouda MN, Varma RS (2013) Greener techniques for the synthesis of silver nanoparticles using plant extracts, enzymes, bacteria, biodegradable polymers, and microwaves. ACS Sustain Chem Eng 1:703–712. https://doi.org/10.1021/sc4000362
19. Skorodumova NV, Simak SI, Lundqvist BI et al (2002) Quantum origin of the oxygen storage capability of ceria. Phys Rev Lett 89:166601. https://doi.org/10.1103/PhysRevLett.89.166601
20. Elahi B, Mirzaee M, Darroudi M et al (2019) Bio-based synthesis of Nano-Ceria and evaluation of its bio-distribution and biological properties. Colloids Surf B 181:830–836. https://doi.org/10.1016/j.colsurfb.2019.06.045
21. Naidi SN, Khan F, Tan AL et al (2021) Green synthesis of CeO_2 and Zr/Sn-dual doped CeO_2 nanoparticles with photoantioxidant and antibiofilm activities. Biomater Sci 9:4854–4869. https://doi.org/10.1039/D1BM00298H
22. Sreekanth TVM, Dillip GR, Lee YR (2016) Picrasma quassioides mediated cerium oxide nanostructures and their post-annealing treatment on the microstructural, morphological and enhanced catalytic performance. Ceram Int 42:6610–6618. https://doi.org/10.1016/j.ceramint.2015.12.171
23. Malleshappa J, Nagabhushana H, Sharma SC et al (2015) Leucas aspera mediated multifunctional CeO_2 nanoparticles: structural, photoluminescent, photocatalytic and antibacterial properties. Spectrochim A 149:452–462. https://doi.org/10.1016/j.saa.2015.04.073
24. Celardo I, Pedersen JZ, Traversa E, Ghibelli L (2011) Pharmacological potential of cerium oxide nanoparticles. Nanoscale 3:1411. https://doi.org/10.1039/c0nr00875c
25. Goubin F, Rocquefelte X, Whangbo M-H et al (2004) Experimental and theoretical characterization of the optical properties of CeO_2, $SrCeO_3$, and Sr_2CeO_4 containing Ce^{4+} (f^0) ions. Chem Mater 16:662–669. https://doi.org/10.1021/cm034618u
26. Jasinski P, Suzuki T, Anderson HU (2003) Nanocrystalline undoped ceria oxygen sensor. Sens Actuators B 95:73–77. https://doi.org/10.1016/S0925-4005(03)00407-6
27. Yao S-Y, Xie Z-H (2007) Deagglomeration treatment in the synthesis of doped-ceria nanoparticles via coprecipitation route. J Mater Process Technol 186:54–59. https://doi.org/10.1016/j.jmatprotec.2006.12.006

28. Ohtake N, Katoh M, Sugiyama S (2017) High thermal-stability ceria synthesized via thermal-hydrolysis route and methane-combustion performance. J Ceram Soc Jpn 125:57–61. https://doi.org/10.2109/jcersj2.16255
29. Kaneko K, Inoke K, Freitag B et al (2007) Structural and morphological characterization of cerium oxide nanocrystals prepared by hydrothermal synthesis. Nano Lett 7:421–425. https://doi.org/10.1021/nl062677b
30. Gharbia N, Elsabbagh S, Saleh A, Hafez H (2022) Green microwave synthesis of ZnO and CeO_2 nanorods for infectious diseases control and biomedical applications. AMB Express 12:153. https://doi.org/10.1186/s13568-022-01495-7
31. Liu Y, Mao D, Yu J et al (2023) Low-temperature CO oxidation on CuO-CeO_2 catalyst prepared by facile one-step solvothermal synthesis: improved activity and moisture resistance via optimizing the activation temperature. Fuel 332:126196. https://doi.org/10.1016/j.fuel.2022.126196
32. Song G, Cheng N, Zhang J et al (2021) Nanoscale cerium oxide: synthesis, biocatalytic mechanism, and applications. Catalysts 11:1123. https://doi.org/10.3390/catal11091123
33. Hussain I, Singh NB, Singh A et al (2016) Green synthesis of nanoparticles and its potential application. Biotechnol Lett 38:545–560. https://doi.org/10.1007/s10529-015-2026-7
34. Gour A, Jain NK (2019) Advances in green synthesis of nanoparticles. Artif Cells Nanomed Biotechnol 47:844–851. https://doi.org/10.1080/21691401.2019.1577878
35. Smuleac V, Varma R, Sikdar S, Bhattacharyya D (2011) Green synthesis of Fe and Fe/Pd bimetallic nanoparticles in membranes for reductive degradation of chlorinated organics. J Membr Sci 379:131–137. https://doi.org/10.1016/j.memsci.2011.05.054
36. Kamatou GP, Vermaak I, Viljoen AM (2012) Eugenol—from the remote maluku islands to the international market place: a review of a remarkable and versatile molecule. Molecules 17:6953–6981. https://doi.org/10.3390/molecules17066953
37. Jirovetz L, Buchbauer G, Stoilova I et al (2006) Chemical composition and antioxidant properties of clove leaf essential oil. J Agric Food Chem 54:6303–6307. https://doi.org/10.1021/jf060608c
38. El-Maati MFA, Mahgoub SA, Labib SM et al (2016) Phenolic extracts of clove (*Syzygium aromaticum*) with novel antioxidant and antibacterial activities. Eur J Integr Med 8:494–504. https://doi.org/10.1016/j.eujim.2016.02.006
39. Tsai T-H, Huang W-C, Lien T-J et al (2017) Clove extract and eugenol suppress inflammatory responses elicited by *Propionibacterium acnes in vitro* and *in vivo*. Food Agric Immunol 28:916–931. https://doi.org/10.1080/09540105.2017.1320357
40. Mahmoodi P, Motavalizadehkakhky A, Darroudi M et al (2023) Green synthesis of cerium oxide nanoparticles using zucchini peel extract for cytotoxic and photocatalytic properties. Bioprocess Biosyst Eng 46:1163–1173. https://doi.org/10.1007/s00449-023-02888-z
41. Tabti HA, Adjdir M, Ammam A et al (2020) Facile synthesis of Cu-LDH with different Cu/Al molar ratios: application as antibacterial inhibitors. Res Chem Intermed 46:5377–5390. https://doi.org/10.1007/s11164-020-04268-8
42. Arumugam A, Karthikeyan C, Haja Hameed AS et al (2015) Synthesis of cerium oxide nanoparticles using *Gloriosa superba* L. leaf extract and their structural, optical and antibacterial properties. Mater Sci Eng C 49:408–415. https://doi.org/10.1016/j.msec.2015.01.042
43. Jafari H, Ganjali MR, Dezfuli AS, Faridbod F (2018) Long term determination of dopamine and uric acid in the presence of ascorbic acid using ytterbia/reduced graphene oxide nanocomposite prepared through a sonochemical route. Appl Surf Sci 427:496–506. https://doi.org/10.1016/j.apsusc.2017.08.054
44. Mahalakshmi S, Hema N, Vijaya PP (2020) In vitro biocompatibility and antimicrobial activities of zinc oxide nanoparticles (ZnO NPs) prepared by chemical and green synthetic route—a comparative study. BioNanoScience 10:112–121. https://doi.org/10.1007/s12668-019-00698-w
45. Li X, Tao R, Xin Y, Lubineau G (2022) Cassette-like peeling system for testing the adhesion of soft-to-rigid assemblies. Int J Solids Struct 251:111751. https://doi.org/10.1016/j.ijsolstr.2022.111751
46. Gerzsenyi TB, Ilosvai ÁM, Szilágyi G et al (2023) A simplified and efficient method for production of manganese ferrite magnetic nanoparticles and their application in DNA isolation. Int J Mol Sci 24:2156. https://doi.org/10.3390/ijms24032156
47. Parvathy S, Manjula G, Balachandar R, Subbaiya R (2022) Green synthesis and characterization of cerium oxide nanoparticles from *Artabotrys hexapetalus* leaf extract and its antibacterial and anticancer properties. Mater Lett 314:131811. https://doi.org/10.1016/j.matlet.2022.131811

48. Ahmed HE, Iqbal Y, Aziz MH et al (2021) Green synthesis of CeO2 nanoparticles from the *Abelmoschus esculentus* extract: evaluation of antioxidant, anticancer, antibacterial, and wound-healing activities. Molecules 26:4659. https://doi.org/10.3390/molecules26154659
49. Anvarinezhad M, Javadi A, Jafarizadeh-Malmiri H (2020) Green approach in fabrication of photocatalytic, antimicrobial, and antioxidant zinc oxide nanoparticles—hydrothermal synthesis using clove hydroalcoholic extract and optimization of the process. Green Process Synth 9:375–385. https://doi.org/10.1515/gps-2020-0040
50. Bensalem A, Muller JC, Bozon-Verduraz F (1992) Faraday communications. From bulk CeO_2 to supported cerium–oxygen clusters: a diffuse reflectance approach. J Chem Soc Faraday Trans 88:153–154. https://doi.org/10.1039/FT9928800153
51. Abhilash MR, Akshatha G, Srikantaswamy S (2019) Photocatalytic dye degradation and biological activities of the Fe_2O_3/Cu_2O nanocomposite. RSC Adv 9:8557–8568. https://doi.org/10.1039/C8RA09929D
52. Vidal F, Eddrief M, Rache Salles B et al (2013) Photon energy dependence of circular dichroism in angle-resolved photoemission spectroscopy of Bi_2Se_3 Dirac states. Phys Rev B 88:241410. https://doi.org/10.1103/PhysRevB.88.241410
53. Lente G (2018) Facts and alternative facts in chemical kinetics: remarks about the kinetic use of activities, termolecular processes, and linearization techniques. Curr Opin Chem Eng 21:76–83. https://doi.org/10.1016/j.coche.2018.03.007
54. Killivalavan G, Sathyaseelan B, Kavitha G et al (2020) Cobalt metal ion doped cerium oxide (Co-CeO_2) nanoparticles effect enhanced photocatalytic activity. MRS Adv 5:2503–2515. https://doi.org/10.1557/adv.2020.296
55. Ranjith KS, Dong C-L, Lu Y-R et al (2018) Evolution of visible photocatalytic properties of Cu-doped CeO_2 nanoparticles: role of Cu^{2+}-mediated oxygen vacancies and the mixed-valence states of Ce ions. ACS Sustain Chem Eng 6:8536–8546. https://doi.org/10.1021/acssuschemeng.8b00848
56. Pathak TK, Coetsee-Hugo E, Swart HC et al (2020) Preparation and characterization of Ce doped ZnO nanomaterial for photocatalytic and biological applications. Mater Sci Eng B 261:114780. https://doi.org/10.1016/j.mseb.2020.114780
57. Choi YI, Kim Y-I, Cho DW et al (2015) Recyclable magnetic $CoFe_2O_4$/BiOX (X = Cl, Br and I) microflowers for photocatalytic treatment of water contaminated with methyl orange, rhodamine B, methylene blue, and a mixed dye. RSC Adv 5:79624–79634. https://doi.org/10.1039/C5RA17616F
58. Tang S, Wang Z, Deling S et al (2020) Enhanced photocatalytic performance of $BiVO_4$ for degradation of methylene blue under LED visible light irradiation assisted by peroxymonosulfate. Int J Electrochem Sci 15:2470–2480. https://doi.org/10.20964/2020.03.09
59. Das GS, Shim JP, Bhatnagar A et al (2019) Biomass-derived carbon quantum dots for visible-light-induced photocatalysis and label-free detection of Fe(III) and ascorbic acid. Sci Rep 9:15084. https://doi.org/10.1038/s41598-019-49266-y
60. Atta AM, Moustafa YM, Al-Lohedan HA et al (2020) Methylene blue catalytic degradation using silver and magnetite nanoparticles functionalized with a poly(ionic liquid) based on quaternized dialkylethanolamine with 2-acrylamido-2-methylpropane sulfonate-*co*-vinylpyrrolidone. ACS Omega 5:2829–2842. https://doi.org/10.1021/acsomega.9b03610
61. Hajipour P, Bahrami A, Eslami A et al (2020) Chemical bath synthesis of CuO-GO-Ag nanocomposites with enhanced antibacterial properties. J Alloys Compd 821:153456. https://doi.org/10.1016/j.jallcom.2019.153456
62. Elshypany R, Selim H, Zakaria K et al (2021) Elaboration of Fe3O4/ZnO nanocomposite with highly performance photocatalytic activity for degradation methylene blue under visible light irradiation. Environ Technol Innov 23:101710. https://doi.org/10.1016/j.eti.2021.101710
63. Ahmed MK, El-Naggar ME, Aldalbahi A et al (2020) Methylene blue degradation under visible light of metallic nanoparticles scattered into graphene oxide using laser ablation technique in aqueous solutions. J Mol Liq 315:113794. https://doi.org/10.1016/j.molliq.2020.113794
64. Arabi A, Fazli M, Ehsani MH (2018) Synthesis and characterization of calcium-doped lanthanum manganite nanowires as a photocatalyst for degradation of methylene blue solution under visible light irradiation. Bull Mater Sci 41:77. https://doi.org/10.1007/s12034-018-1590-6
65. Xia T, Kovochich M, Liong M et al (2008) Comparison of the mechanism of toxicity of zinc oxide and cerium oxide nanoparticles based on dissolution and oxidative stress properties. ACS Nano 2:2121–2134. https://doi.org/10.1021/nn800511k
66. Chandraker SK, Kumar R (2022) Biogenic biocompatible silver nanoparticles: a promising antibacterial agent. Biotechnol Genet Eng Rev. https://doi.org/10.1080/02648725.2022.2106084

67. Nguyen THA, Nguyen V-C, Phan TNH et al (2022) Novel biogenic silver and gold nanoparticles for multifunctional applications: green synthesis, catalytic and antibacterial activity, and colorimetric detection of Fe(III) ions. Chemosphere 287:132271. https://doi.org/10.1016/j.chemosphere.2021.132271
68. Munawar T, Mukhtar F, Nadeem MS et al (2020) Novel photocatalyst and antibacterial agent; direct dual Z-scheme ZnO–CeO_2-Yb_2O_3 heterostructured nanocomposite. Solid State Sci 109:106446. https://doi.org/10.1016/j.solidstatesciences.2020.106446
69. Eka Putri G, Rilda Y, Syukri S et al (2021) Highly antimicrobial activity of cerium oxide nanoparticles synthesized using *Moringa oleifera* leaf extract by a rapid green precipitation method. J Mater Res Technol 15:2355–2364. https://doi.org/10.1016/j.jmrt.2021.09.075

Authors and Affiliations

Brahim Djemoui[1] · Samia Gharbi[2] · Choukry Kamel Bendeddouche[1] · Zohra Taibi[3] · Miloud Mohamed Mazari[1] · Abdelhalim Zoukel[4] · Noureddine Karkachi[5] · Mehdi Adjdir[1,6]

✉ Mehdi Adjdir
mehdi.adjdir@daad-alumni.de

[1] Laboratory of Applied Organic Synthesis, Faculty of Exact and Applied Sciences, University Oran 1 Ahmed Ben Bella, El M'Naouer, BP 1524, 31000 Oran, Algeria

[2] Department of Biotechnology, University of Science and Technology of Oran Mohamed Boudiaf, Oran, Algeria

[3] Laboratoire Physico-Chimie des Matériaux-Catalyse et Environnement (LPCMCE), Université des Sciences et de la Technologie d'Oran Mohamed Boudiaf (USTOMB), El M'naouer, BP 1505, 31000 Oran, Algeria

[4] Platform of Physico-Chemical Analysis (PTAPC-Laghouat-CRAPC), Laghouat, Algeria

[5] Laboratory of Applied Microbiology, Department of Biology, Faculty of Natural and Life Sciences, University of Oran 1 Ahmed Ben Bella, El M'naouer, BP 1524, 31000 Oran, Algeria

[6] Department of Engineering Process, Faculty of Technology, Dr Moulay Taher University, Ennasr, BP 138, 20000 Saida, Algeria